International Journal on Magnetic Particle Imaging
Vol 11, No 1, Article ID 2508003, 8 Pages

Infinite Science Publishing

Research Article

Phase-sensitive signal processing in the DiffMag handheld probe

Thom van Ommeren [a] · Sebastiaan Waanders [a] · Tom Trapman [a] · Erik Krooshoop [a] · Bennie ten Haken [a] · Lejla Alic [a,*]

[a] Magnetic Detection & Imaging Group, Technical Medical Centre, University of Twente, Enschede, The Netherlands
*Corresponding author, email: LejlaResearch@gmail.com

Received 01 November 2024; Accepted 02 June 2025; Published online 26 August 2025

Abstract

Sentinel Lymph Node Biopsy (SLNB) is a surgical procedure that employs a tracer and a handheld detection device to assess lymphatic metastasis. Superparamagnetic iron oxide nanoparticles (SPIONs) have been used as tracers, with handheld magnetometers utilised for detection. The differential magnetometry processing technique (DiffMag) effectively suppresses interference from stationary magnetic materials. However, movement of magnetic materials introduces signal artefacts—referred to as motion artefact—due to the sequential nature of the processing technique. Continuous manoeuvring of surgical equipment during SLNBs generates such artefact, potentially extending surgery time. To address this drawback, we propose an extension of DiffMag using phase-sensitive signal processing to measure phase lag—a property unique to signals from SPIONs. This extension demonstrates potential to differentiate SPION signals from motion artefacts. In this study, we examined phase lag across various SPION types (Magtrace, Resotran, Resovist, Ferrotrace) within clinically relevant parameter for SLNB, including low SPION concentrations and increased environmental viscosity. Implementing the processing technique in the DMH yielded highly stable phase measurements characterised by low noise levels and negligible drift. Notably, SPIONs across all tested conditions exhibited a distinct measurable phase difference to those of motion artefacts. In conclusion, phase-sensitive signal processing utilised in the DMH-probe demonstrates strong potential for differentiating SPION signals from motion artefacts.

I. Introduction

Lymph node (LN) metastasis, particularly involving the LN directly connected to the primary tumour—referred to as the sentinel LN (SLN)—serves as a key indicator for disease progression, staging, and treatment stratification [1]. To evaluate metastatic dissemination, the sentinel lymph node biopsy (SLNB) procedure was developed, wherein the SLN is surgically excised and assessed for metastatic involvement [2]. This technique relies on the administration of a tracer and the use of a handheld detection device to localise the SLN. Superparamagnetic iron oxide nanoparticles (SPIONs), have emerged as promising tracers for SLN localisation owing to their favourable non-linear magnetic characteristics [3, 4]. Endomagnetics (Cambridge, United Kingdom) offers a CE-marked and FDA approved combination product that includes a SPION tracer and a handheld magnetometer [5]. This conventional magnetometer measures the net magnetic susceptibility of all materials within its scan volume, accounting not only for the superparamagnetic signal from SPIONs but also confounding signals

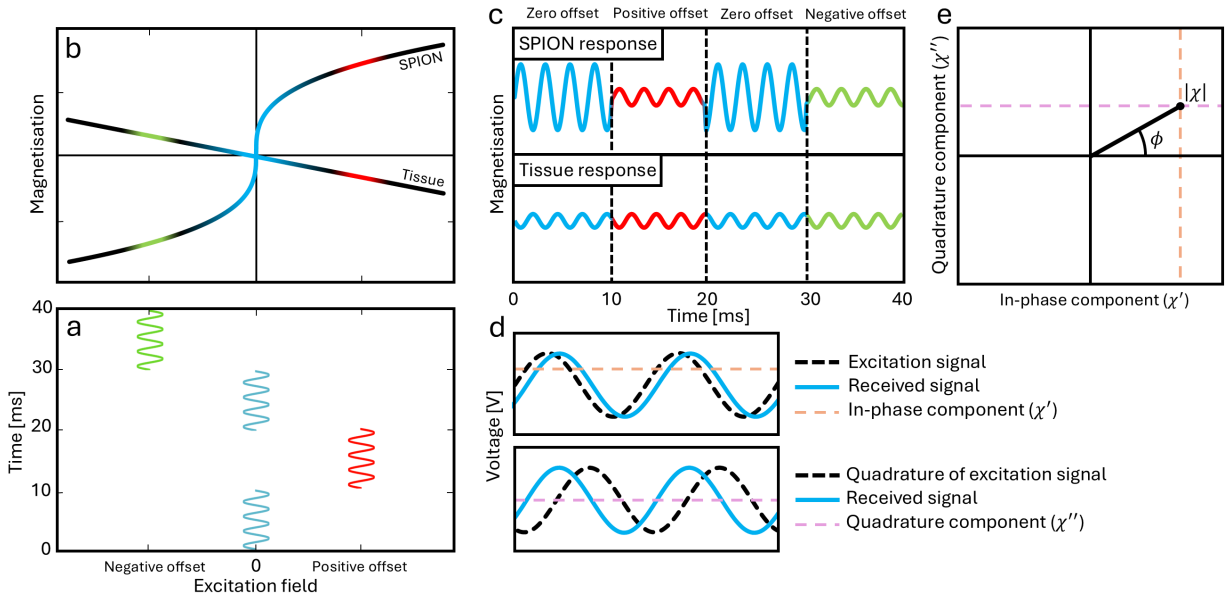

Figure 1: The DiffMag sensing principle and phase-sensitive signal processing visualised for a single hypothetical duty cycle. **a:** The excitation magnetic field consisting of an AC field with an alternating three-level offset which creates a positive and a negative offset field. **b:** The magnetisation curves of SPIONs and tissue, not to scale. The colours indicate the location of the offsets on the curve. **c:** The magnetisation response of SPIONs and tissue in the presence and absence of an offset. The non-linear magnetic susceptibility of SPIONs results in a reduced magnetisation response during offset, while biological tissue displays a constant magnetisation response regardless of the offset level. **d:** Multiplication and averaging of the received voltage signal with the reference signal yields and the quadrature of the reference signal results in the in-phase component χ' and the quadrature component χ'' respectively. **e:** The relation between χ' and χ'' in the Cartesian coordinate system and the phase lag ϕ_p in the polar coordinate system are given, revealing the inverse tangent relation between the phase lag and both components.

from diamagnetic tissue and paramagnetic and ferromagnetic materials, such as surgical instruments [6]. To mitigate magnetic interference, the use of non-metallic surgical instruments during SLNB is recommended; however, this introduces additional complexity to the surgical procedure and prolongs the surgery time, thereby limiting its clinical practicality [7].

Differential magnetometry (DiffMag) is a patented processing technique [8] developed at the University of Twente for selective detection of SPIONs within the human body [6, 9–11]. This method overcomes several limitations of conventional magnetometers by exploiting the non-linear magnetic susceptibility characteristic of SPIONs, enabling their discrimination from surrounding biological tissue [6]. DiffMag combines a sinusoidal alternating field (AC-field) superimposed with an alternating three-level offset for excitation of the SPIONs, as depicted in Figure 1a. In the absence of the offset (zero offset), SPIONs exhibit a markedly higher magnetic susceptibility compared to their response during the offset pulse. In contrast, biological tissue displays a linear susceptibility regardless of the offset level, as illustrated in Figure 1b. Consequently, the signal originating from SPIONs diminishes during the offset periods, while the tissue signal remains unchanged, see Figure 1c. By subtracting the signal acquired during an offset period from the signal acquired during the zero-offset period, the tissue contribution is effectively cancelled, isolating the SPION-specific response. The resulting signal is then averaged over one duty cycle (0.4 s) and discretised in increments of 100 nanovolts. This quantised value is referred to as a DiffMag count, serving as a surrogate marker for SPION concentration [9].

The DiffMag processing technique is integrated into the DiffMag handheld (DMH) probe, a prototype device consisting of a probe, base unit, and the DiffMag processing software, shown in Figure 2. The DiffMag principle effectively eliminates contributions from stationary dia-, para-, or ferromagnetic materials within the DMH probe. However, due to the sequential nature of the DiffMag principle, any movement that alters the magnitude of the measured signal will cause discrepancies between the offset and no-offset states, resulting in artificial changes in the DiffMag signal. These artefacts, resulting from movement-induced changes, are referred to as motion artefacts.

In clinical practice, continuous manoeuvring of surgical equipment is expected to cause motion artefacts. These artefacts appear as transient spikes in the DiffMag counts, marked in red in Figure 3a, and predominantly influence the DiffMag counts during movement of either the probe or metallic equipment. While the

10.18416/ijmpi.2025.2508003

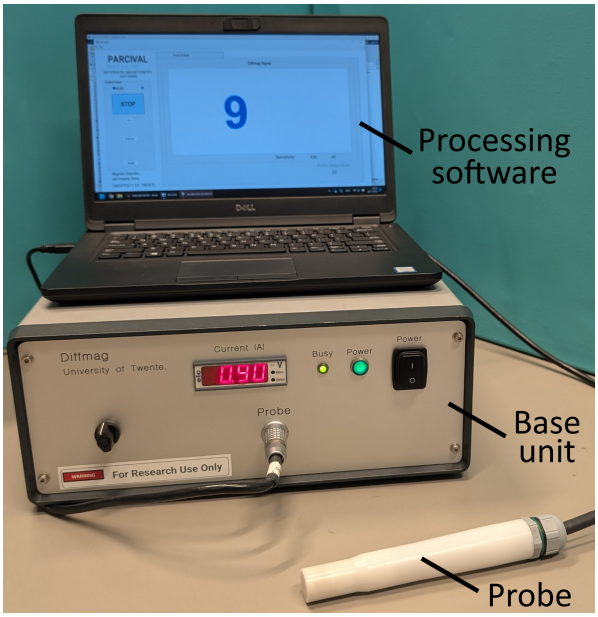

Figure 2: The prototype DiffMag handheld probe with a probe, a base unit, and processing software.

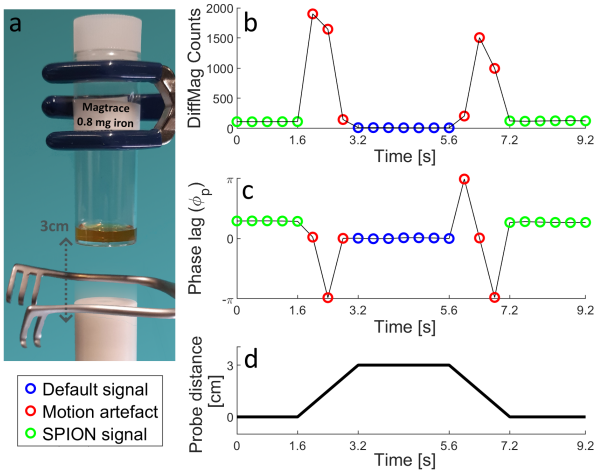

Figure 3: A simulation of motion artefacts by moving the DMH probe through a metal retractor towards a container with 0.8 mg Magtrace. **a:** The experimental setup where the probe was moved a total of three centimetre at a velocity of 100 mm s^{-1}. The effect of motion artefacts in **b:** the DiffMag counts, **c:** the phase lag. SPION measurements are highlighted in green, representing their distinct phase lag values. The absence of any superparamagnetic material in the scanning range is indicated in blue, showing minimal signal and no phase lag. Motion artefacts are highlighted in red, exhibiting DiffMag counts significantly higher than the default signal without exhibiting any phase lag or displaying phase lag values that exceed the typical phase lag of SPIONs. **d:** The distance between the probe and the container over time.

artefacts are short-lived, they are nonetheless disruptive and may prolong surgery duration. To mitigate these challenges, the DiffMag principle has been extended to incorporate phase-sensitive signal processing [6], which facilitates measurements of the unique relaxation behaviour of SPIONs know as phase lag. Preliminary phase measurements obtained using this processing technique, as presented in Figure 3c, demonstrate that phase lag from SPIONs can be effectively distinguished from motion artefacts, which either lack phase signals or exhibit values of $\pm\pi$. Consequently, phase-sensitive signal processing holds promise for differentiating SPION signals from motion artefacts. In this paper, we specifically focus on the phase lag generated by particles and assess the limitations of phase-sensitive signal processing within clinically relevant parameter ranges for SLNB, including low SPION concentrations and elevated viscosities.

II. Theory

When submitted to a magnetic field, a SPION is uniformly magnetised and its magnetic moments aligns with the magnetic field. The magnetic moment naturally aligns with an easy axis, which is an energetically favourable direction caused by magnetic anisotropy. The easy access has two such favourable directions which are opposite of each other. These directions are separated by an energy barrier $\Delta E = K V_c$ where K is the anisotropy constant and V_c is the magnetic core volume. For SPIONs with smaller core sizes, this energy barrier is sufficiently low for thermal fluctuations to cross this energy barrier. This process is called Néel relaxation and the average time between two consecutive flips is called the zero-field Néel relaxation time [12] and is given by:

$$\tau_N = \tau_0 \exp\left(\frac{K V_c}{k_B T}\right), \tag{1}$$

where τ_0 is material characteristic called attempt time, k_B is the Boltzmann's constant, and T is the absolute temperature.

In most SPION applications such as the SNLB, SPIONs are diffused in a liquid forming a ferrofluid. In such fluids, physical rotation of the entire SPION is possible, allowing for a second relaxation mechanism called Brownian relaxation [13]. Brownian relaxation is the physical rotation of the magnetic moment along with the SPION itself. The zero-field Brownian relaxation time is expressed as:

$$\tau_B = \frac{3\eta V_H}{k_B T}, \tag{2}$$

which is governed by the hydrodynamic volume V_H of the particle and the environmental viscosity η.

In most cases, τ_B and τ_N differ by several orders of magnitude [14]. The relaxation process with the shortest relaxation time dominates the observed signal. However, when τ_B and τ_N relaxation times are comparable, both will play a contributing role [15]. Within the assumption that the Néel and Brownian relaxation processes

10.18416/ijmpi.2025.2508003

are independent, the SPION magnetic dynamics is then described through an effective relaxation time τ [16]:

$$\tau = \frac{\tau_N \tau_B}{\tau_N + \tau_B}. \tag{3}$$

When a SPION is re-excited before it has fully restored its magnetic moment—specifically, when the excitation frequency exceeds the effective relaxation time—the relaxation mechanisms are unable to respond adequately to the rapidly alternating field. In such scenarios, the magnetic moment is considered to lag behind the external magnetic field, a phenomenon known as phase lag ϕ_p. Phase lag results in a complex magnetic susceptibility $\tilde{\chi}$ which is described by the Debye model [16–18]:

$$\tilde{\chi}(\omega) = \frac{\chi_0}{1 + i\omega\tau}, \tag{4}$$

where χ_0 is the static magnetic susceptibility and ω is the excitation frequency. The Debye model is strictly valid only for small magnetic fields but can be used to extend the Langevin model, which models the non-linear magnetic susceptibility of SPIONs, into the non-linear range [19]. The complex magnetic susceptibilities has a real component

$$\chi' = \Re(\tilde{\chi}) = \frac{1}{1 + (\omega\tau)^2}\chi_0, \tag{5}$$

and an imaginary component

$$\chi'' = \Im(\tilde{\chi}) = \frac{\omega\tau}{1 + (\omega\tau)^2}\chi_0. \tag{6}$$

Together they describe the magnetic susceptibility in a Cartesian coordinate system, as illustrated in Figure 1e. However, this coordinate system can be converted to polar coordinate system with the modulus of $\tilde{\chi}$ represented as

$$|\tilde{\chi}| = \frac{\chi_0}{\sqrt{1 + (\omega\tau)^2}}, \tag{7}$$

and the phase lag follows from the angle between the two components which results in the following relation between the relaxation time and the phase lag ϕ_p [16]:

$$\phi_p = \tan^{-1}\left(\frac{\chi''}{\chi'}\right) = \tan^{-1}(\omega\tau). \tag{8}$$

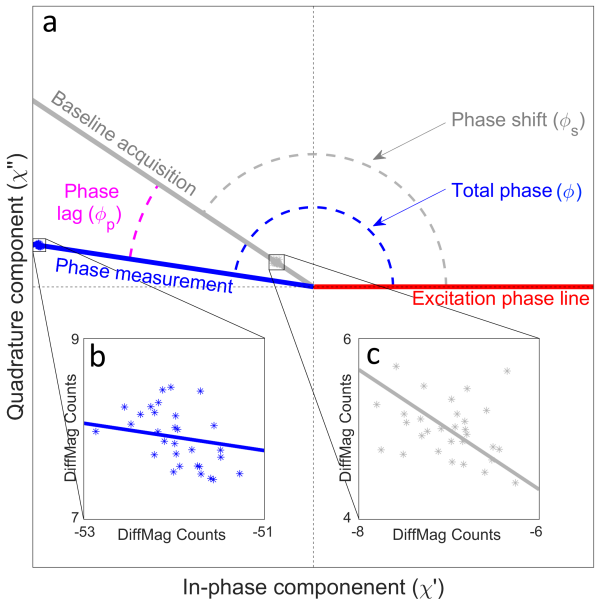

Figure 4: Phase contributions during phase acquisitions. In red the phase of the excitation signal which is set to zero phase. In blue a phase acquisition in the presence of SPIONs. It contains both phase lag ϕ_p and phase shift ϕ_s contributions, indicated in grey and magenta respectively. Subfigures **b** and **c** display thirty consecutively phase acquisitions, illustrating noise characteristics of the DMH probe in the presence of 2 mg Resovist and during a baseline acquisition, respectively. Phase lines are plotted from the origin to the mean phase value of each acquisition set.

III. Materials and Methods

III.I. Phase-sensitive signal processing

Phase-sensitive signal processing employs the real and imaginary components of magnetic susceptibility to digitally compute the phase lag [9]. By feeding the excitation signal back into the processing unit, the system performs a comparative analysis with the received signal, as depicted in Figure 1d, to extract the in-phase and quadrature components. These components are subsequently used to determine the phase lag according to Equation (8), the results of which are illustrated in Figure 1e.

Minor variations in coil geometry and imperfections in electrical components within the feedback system introduce a phase in the reference signal [6, 9]. Consequently, the total phase ϕ measured through phase-sensitive signal processing, illustrated in Figure 4a, consists of both the particle contributed phase lag and the system contributed phase shift ϕ_s. Therefore, thorough understanding of phase shift factors such as consistency, heating effects, drift and noise is essential.

SPIONs	d_H (nm)	d_c (nm)
Magtrace	60 [20]	4.8 [20]
Resotran	66 [21]	3.3 [21]
Resovist	56 [21]	4.0 [21]
Ferrotrace	74 [22]	16 [22]

Table 1: Average hydrodynamic diameter d_H and core diameter d_c of Magtrace, Resotran, Resovist, Ferrotrace.

III.II. Samples

Four different SPIONs: Magtrace® (EndoMag, UK), Resotran® (Bayer Schering Pharma GmbH, Germany), Resovist® (Kyowa CritiCare, Japan), and Ferrotrace® (Ferronova, Australia) with corresponding sizes presented in Table 1 were used for all experiments.

Two series of samples were prepared to evaluate the effect of varying concentration and viscosity on the performance of phase-sensitive signal processing. In the dilution series, decreasing amounts of iron ranging from 1400 µg iron to 10 µg iron were used, encompassing the clinically relevant amount of 20 µg iron typically observed in SLNs [23]. In the viscosity series, increasing amounts of glycerol (0, 250, 500, 750, and 1000 µl) were added to a fixed amount of 1400 µg iron. All samples were filled to a total sample volume of 1.5 ml using deionised water, yielding estimated dynamic viscosities of 1.0, 1.7, 3.4, 8.4, and 26.6 mPa s receptively at 20 °C [24]. These viscosities were chosen for both clinical relevance and system limitations. According to the literature, the viscosity of lymph at 37 °C is 1.7 mPa s [25], however, the biological environment surrounding SPIONs in LNs may restrict particle motion, thereby partially or completely impeding the Brownian relaxation mechanism [20, 26]. Consequently, higher viscosities were chosen to assess system feasibility when Brownian relaxation is partially or fully inhibited.

III.III. Data acquisition

Experiment I: phase shift. The DMH probe was used to assess the phase shift by acquiring baseline data over four consecutive days, directly after starting up the system, with the probe stabilised at a consistent probe temperature of 20.0 °C. Each individual acquisition was recorded at an excitation frequency of 2.5 kHz during 30 consecutive duty cycles. One additional measurement consisting of 90 consecutive duty cycles was conducted to investigate potential drift in phase shift.

To examine the effects of probe temperature on system phase shift, prior to data acquisition, the probe was cooled to 10.6 °C and subsequently heated to 42.2 °C, both using a water bath. After reaching these temperatures, the probe was allowed to gradually stabilise to laboratory temperature of 20 °C, and phase data was acquired during this stabilisation period for 30 consecutive duty cycles every 60 seconds. The build-in temperature sensor in the probe was used for simultaneous temperature acquisition.

Experiment II: phase lag. For both sample series, phase data was recorded using the DMH probe at 2.5 kHz over 30 consecutive duty cycles at laboratory temperature of 20 °C. For each sample, the plastic sample container was placed directly on top of the DMH probe (Figure 5c). Data included a baseline acquisition to assess the phase shift prior to sample placement, followed by individual acquisition for each sample. One additional measurement consisting of 90 consecutive duty cycles was conducted to investigate potential drift in the phase lag.

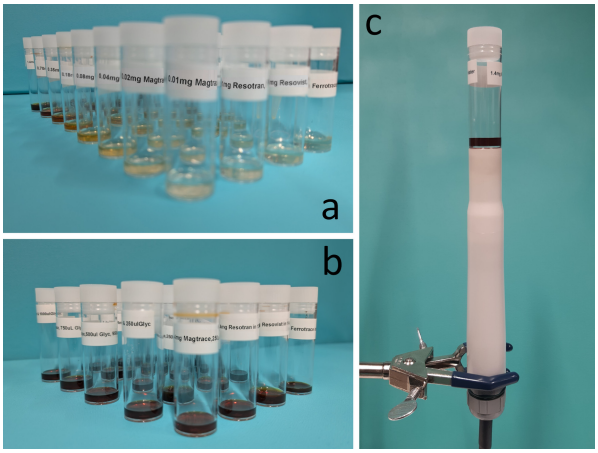

Figure 5: **a:** A dilution series of Magtrace, Resotran, Resovist, and Ferrotrace containing 1.40, 0.70, 0.35, 0.18, 0.08, 0.04, 0.02, and 0.01 mg iron. All samples are diluted with deionised water to a total volume of 1.5 ml. **b:** A viscosity series of the same set of SPIONs containing 1.40 mg iron and 0, 250, 500, 750, and 1000 µl glycerol. All samples diluted with deionised water to a total volume of 1.5 ml. **c:** Data acquisition by placing the plastic sample container directly on top of the DMH probe.

III.IV. Data processing

For each acquisition, the measured phase was determined by averaging 30 consecutive measurements. The baseline phase shift, established in Experiment I, served as a reference for evaluating the phase lag in subsequent concentration and viscosity experiments. In Experiment II, the phase lag was obtained by subtracting the baseline phase shift from the averaged total phase.

Phase noise was assessed in the Cartesian coordinate system rather than the polar coordinate system due to the substantial phase uncertainty expected near the origin in polar coordinate systems [27]. To evaluate phase noise, a linear fit was applied between the origin and the cluster of measurements, as illustrated in Figure 4b. Noise magnitude was quantified by computing the standard deviation of the orthogonal distances from individual data points to the fitted phase line, expressed in DiffMag counts. The distribution of these deviations was subsequently analysed for normality using the Shapiro-Wilk test.

IV. Results

Experiment I: phase shift. The average phase shift recorded in 21 baseline acquisitions acquired over

various days and probe temperatures was 2.570 ± 0.016 rad. As illustrated in Figure 6c, probe heating from 10.6 to 42.2 °C lead to a non-linear increase in system phase shift, of approximately $4.5 \cdot 10^{-3}$ rad. For all 21 baseline acquisitions, the average phase noise was 0.1535 ± 0.0408 DiffMag counts. The Shapiro-Wilk Test indicated that the noise in 19 out of 21 baseline acquisitions followed a normal distribution. Additionally, no phase drift was observed in any of the baseline acquisitions.

Experiment II: phase lag. Figure 6 presents the measured phase lags across the dilution and viscosity series for each sample. For iron concentration of 80 µg or greater without added glycerol, Magtrace, Resotran, Resovist, and Ferrotrace exhibited distinct phase lags of 0.422 ± 0.002, 0.450 ± 0.002, 0.347 ± 0.001, and 1.038 ± 0.010 rad respectively. Phase lag was detectable for all SPION types down to 10 µg iron; however, a reduction in phase lag was observed at lower concentrations, as illustrated in Figure 6a. Specifically, comparing 10 µg to 1400 µg iron, Magtrace, Resotran, Resovist, and Ferrotrace exhibited respective decreases of 0.192, 0.230, 0.201, and 0.213 rad, corresponding to relative reductions of 19.21%, 23.01%, 20.10%, and 21.34%.

Magtrace, Resotran, and Resovist exhibit comparable trends in response to increasing viscosity, characterised primarily by a reduction in phase lag, as depicted in Figure 6b. As viscosity increased from 1.0 to 1.7 mPa s, the phase lag decreased by 26.9%, 25.5%, and 25.5% for Magtrace, Resotran, and Resovist, respectively. In contrast, Ferrotrace demonstrated a divergent response, with a slight increase of 2.5% over the same viscosity range. At higher viscosities, however, all four SPION types displayed a consistent trend of decreasing phase lag. An increase in viscosity from 1.0 to 26.6 mPa s led to reductions of 67.6%, 70.3%, 69.0%, and 66.7% for Magtrace, Resotran, Resovist, and Ferrotrace, respectively.

For all 48 samples in the dilution and viscosity series, the average phase noise was 0.2409 ± 0.1252 DiffMag counts. The Shapiro-Wilk Test indicated that 47 out of 48 baseline acquisitions experienced normally distributed noise. Throughout the acquisition process, a slight phase drift of 8×10^{-5} rad s^{-1} was observed in all SPIONs, with an example of this drift illustrated in Figure 6d.

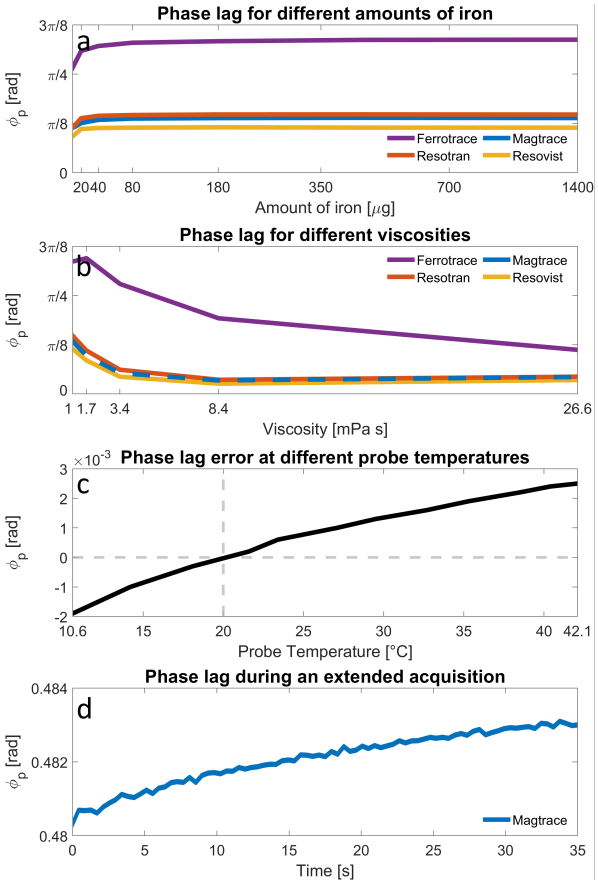

Figure 6: **a:** Phase lag acquisitions of four different SPIONs: Magtrace, Resotran, Resovist, and Ferrotrace for a dilution series ranging from 10 µg to 1400 µg iron. **b:** Phase lag acquisitions of 1400 µg iron for the same set of particles for a viscosity series. **c:** Phase lag errors as the probe temperature deviates from laboratory temperature of 20 °C. **d:** An extended phase lag acquisition of 1400 µg Magtrace.

V. Discussion

In this study, we demonstrated the capability to measure phase lag using a handheld magnetometer at clinically relevant concentrations (20 µg) and viscosities of 1.7 mPa s and above. The results indicate that SPIONs consistently exhibit a detectable phase difference relative to baseline acquisitions under all tested conditions, indicating the ability to distinguish SPIONs from motion artefacts in clinically relevant conditions. Among the tested particles, Magtrace, Resotran, and Resovist show highly similar phase lags, with only minor variations attributable to their comparable, yet slightly differing, hydrodynamic and core diameters. In contrast, Ferrotrace consistently exhibits significantly different phase lag values, which can be attributed to its substantially larger hydrodynamic and core size compared to the other particles.

Lower iron concentrations and increasing viscosities were observed to decrease the phase lag, which contradicts the theoretical predictions presented in this study. It is important to acknowledge that Equations (1) and (2) represent simplified models of the relaxation behaviour, as they assume non-interacting SPIONs and are based on the zero-field scenario—specifically, the situation when an applied external magnetic field is abruptly removed. Moreover, the models do not account for SPION relaxation within AC fields, as employed in the DMH. It is well established that SPIONs exhibit more complex

phase lag behaviour under such external fields, requiring more sophisticated modelling approaches [28, 29]. Consequently, these models do not consider inter-particle interactions, such as coating interactions [30], which may have a reduced effect at lower concentrations.

Comparable findings were reported by Utkur et al. [31], who observed a decrease in relaxation time with increasing viscosity. The authors suggested that differences in the chemical environment between the water solution and the water/glycerol mixture may cause this behaviour—affecting inter-particle interactions or interactions with the surrounding medium. Although the applied models were unable to accurately predict the phase lag behaviour, it is important to note that this was not the primary objective of the study. Instead, the most significant outcome is the consistent measurement of a distinct phase difference compared to the baseline acquisition across all tested conditions. This finding is particularly important as it highlights the potential of phase-sensitive signal processing to differentiate SPIONs from motion artefacts in clinical settings.

The implementation of the processing technique within the DMH probe yielded highly stable phase measurements, characterised by low noise levels and negligible drift. The observed noise exhibited an additive profile, as evidenced by the comparable noise levels in both the baseline and sample acquisition. Statistical evaluation using the Shapiro-Wilk Test confirmed that the noise distribution conforms to normality.

Notably, non-linear phase drift was exclusively detected during sample acquisitions, and was absent in baseline acquisitions, suggesting particle-specific origin. Potential contributors to this drift include localised heating within the AC field [32] or thermal energy transfer between the probe and the container as the probe warms. Such temperature changes can influence magnetic relaxation mechanisms. Although Equations (1) and (2) predict a reduction in phase lag with increasing temperatures, the experimental observations demonstrated an opposing trend. This inconsistency may reflect the limitations and oversimplifications in the underlying relaxation models. Nevertheless, the findings reported by He et al. were consistent with theoretical expectations, supporting a temperature-dependent reduction in relaxation time [33].

Despite the uncertainty surrounding the exact cause of the phase drift, its impact on phase measurements appears minimal due to its relatively small magnitude. Further investigation into the mechanisms underlying this non-linearity could provide valuable insights for optimising system performance and enhancing the accuracy of phase-sensitive signal processing in practical applications. Additionally, it highlights the need to explore the influence of body temperature on the phase lag of particles. However, since the literature suggest that phase lag persists at elevated temperatures [34], it is believed that a distinct phase difference from the baseline acquisition would still be detectable.

Furthermore, performing a multivariate analysis that integrates clinically relevant concentrations, viscosities, and temperatures could offer a more comprehensive evaluation of the clinical feasibility of phase-sensitive signal processing. While the phase lag at the edge cases of both low concentrations and high viscosities were measurable, and temperature is also expected to be measurable, predicting detectability of phase lag when all three variables are combined remains challenging. While models are available that can estimate relaxation times in these scenarios, translating these estimates directly to phase detectability in the DMH is not straightforward and warrants further investigation.

VI. Conclusion

Phase-sensitive signal processing demonstrates strong potential for differentiating SPIONs from metallic instruments by leveraging their distinct relaxation characteristics. Consistent and distinct phase difference compared to the baseline acquisition across low iron concentrations and higher viscosities highlight the potential of phase-sensitive signal processing for clinical applications. Further research is required to examine phase lag at body temperatures. Additionally, investigating the underlying mechanisms contributing to the observed nonlinearity and the increase in system phase shift with temperature will provide valuable insights for optimising system performance and enhancing accuracy.

Author's statement

The authors presented this work under the same title at IWMPI 2025. Authors state no conflict of interest. Informed consent has been obtained from all individuals included in this study.

References

[1] T. P. Padera, E. F. Meijer, and L. L. Munn. The Lymphatic System in Disease Processes and Cancer Progression. *Annual review of biomedical engineering*, 18:125–158, 2016, doi:10.1146/annurev-bioeng-112315-031200.

[2] M. K. Kim, H. S. Park, J. Y. Kim, S. Kim, S. Nam, S. Park, and S. I. Kim. The clinical implication of the number of lymph nodes harvested during sentinel lymph node biopsy and its effects on survival outcome in patients with node-negative breast cancer. *American journal of surgery*, 214(4):726–732, 2017, doi:10.1016/j.amjsurg.2016.10.019.

[3] J. J. Pouw, M. R. Grootendorst, J. M. Klaase, J. van Baarlen, and B. ten Haken. Ex vivo sentinel lymph node mapping in colorectal cancer using a magnetic nanoparticle tracer to improve staging accuracy: a pilot study. *Colorectal Disease*, 18(12):1147–1153, 2016, doi:10.1111/codi.13395.

[4] L. Molenaar, M. M. Van De Loosdrecht, L. Alic, J. Van Baarlen, J. J. Meijerink, B. T. Haken, I. A. Broeders, and D. J. Lips. Quantification of Magnetic Nanoparticles in ex vivo Colorectal Lymph Nodes. *Nano LIFE*, 12(3), 2022, doi:10.1142/S1793984422500064.

[5] M. Douek, J. Klaase, I. Monypenny, A. Kothari, K. Zechmeister, D. Brown, L. Wyld, P. Drew, H. Garmo, O. Agbaje, Q. Pankhurst, B. Anninga, M. Grootendorst, B. Ten Haken, M. A. Hall-Craggs, A. Purushotham, and S. Pinder. Sentinel node biopsy using a magnetic tracer versus standard technique: the SentiMAG Multicentre Trial. *Annals of surgical oncology*, 21(4):1237–1245, 2014, doi:10.1245/s10434-013-3379-6.

[6] M. Visscher, S. Waanders, H. J. Krooshoop, and B. ten Haken. Selective detection of magnetic nanoparticles in biomedical applications using differential magnetometry. *Journal of Magnetism and Magnetic Materials*, 365:31–39, 2014, doi:10.1016/j.jmmm.2014.04.044.

[7] A. Piñero-Madrona, J. A. Torró-Richart, J. M. De León-Carrillo, G. De Castro-Parga, J. Navarro-Cecilia, F. Domínguez-Cunchillos, J. M. Román-Santamaría, C. Fuster-Diana, and R. Pardo-García. Superparamagnetic iron oxide as a tracer for sentinel node biopsy in breast cancer: A comparative non-inferiority study. *European journal of surgical oncology*, 41(8):991–997, 2015, doi:10.1016/j.ejso.2015.04.017.

[8] S. Waanders, M. Visscher, T. O. B. Oderkerk, H. J. G. Krooshoop, and B. ten Haken, Method and apparatus for measuring an amount of superparamagnetic material in an object, 2018.

[9] S. Waanders, M. Visscher, R. R. Wildeboer, T. O. Oderkerk, H. J. Krooshoop, and B. ten Haken. A handheld SPIO-based sentinel lymph node mapping device using differential magnetometry. *Physics in Medicine and Biology*, 61(22), 2016, doi:10.1088/0031-9155/61/22/8120.

[10] S. Salamzadeh, H. J. Krooshoop, B. ten Haken, and L. Alic. DiffMag handheld probe for perioperative lymph node harvesting. *International Journal on Magnetic Particle Imaging IJMPI*, 9(1 Suppl 1), 2023, doi:10.18416/ijmpi.2023.2303052.

[11] E. R. Nieuwenhuis, N. Mir, M. M. Horstman-van de Loosdrecht, A. P. Meeuwis, M. G. de Bakker, T. W. Scheenen, and L. Alic. Performance of a Nonlinear Magnetic Handheld Probe for Intraoperative Sentinel Lymph Node Detection: A Phantom Study. *Annals of Surgical Oncology*, 30(13):8735, 2023, doi:10.1245/S10434-023-14166-Z.

[12] L. Néel. Théorie du traînage magnétique des ferromagnétiques en grains fins avec application aux terres cuites. *Annales de géophysique*, 5:99–136, 1949.

[13] W. F. Brown. Thermal Fluctuations of a Single-Domain Particle. *Physical Review*, 130(5):1677–1686, 1963, doi:10.1103/PhysRev.130.1677.

[14] I. M. Perreard, D. B. Reeves, X. Zhang, E. Kuehlert, E. R. Forauer, and J. B. Weaver. Temperature of the magnetic nanoparticle microenvironment: estimation from relaxation times. *Physics in Medicine & Biology*, 59(5):1109, 2014, doi:10.1088/0031-9155/59/5/1109.

[15] K. Wu, L. Tu, D. Su, and J.-P. Wang. Magnetic dynamics of ferrofluids: mathematical models and experimental investigations. *Journal of Physics D: Applied Physics*, 50(8):85005, 2017, doi:10.1088/1361-6463/aa590b.

[16] R. E. Rosensweig. Heating magnetic fluid with alternating magnetic field. *Journal of Magnetism and Magnetic Materials*, 252(1-3 SPEC. ISS.):370–374, 2002, doi:10.1016/S0304-8853(02)00706-0.

[17] P. Debye. Zur Theorie der spezifischen Wärmen. *Annalen der Physik*, 344(14):789–839, 1912, doi:10.1002/ANDP.19123441404.

[18] M. I. Shliomis and Y. L. Raikher. Experimental investigations of magnetic fluids. *IEEE Transactions on Magnetics*, 16(2):237–250, 1980, doi:10.1109/TMAG.1980.1060590.

[19] T. Wawrzik, T. Yoshida, M. Schilling, and F. Ludwig. Debye-Based Frequency-Domain Magnetization Model for Magnetic Nanoparticles in Magnetic Particle Spectroscopy. *IEEE Transactions on Magnetics*, 51(2):5300404, 2015, doi:10.1109/TMAG.2014.2332371.

[20] K. Riahi, M. M. van de Loosdrecht, L. Alic, and B. ten Haken. Assessment of differential magnetic susceptibility in nanoparticles: Effects of changes in viscosity and immobilisation. *Journal of Magnetism and Magnetic Materials*, 514:167238, 2020, doi:10.1016/J.JMMM.2020.167238.

[21] F. Mohn, K. Scheffler, J. Ackers, A. Weimer, F. Wegner, F. Thieben, M. Ahlborg, P. Vogel, M. Graeser, and T. Knopp. Characterization of the clinically approved MRI tracer resotran for magnetic particle imaging in a comparison study. *Physics in medicine and biology*, 69(13), 2024, doi:10.1088/1361-6560/AD5828.

[22] G. Krishnan, A. Cousins, N. Pham, V. Milanova, M. Nelson, S. Krishnan, A. Shetty, N. van den Berg, E. Rosenthal, S. Krishnan, P. J. Wormald, A. Foreman, and B. Thierry. Preclinical evaluation of a mannose-labeled magnetic tracer for enhanced sentinel lymph node retention in the head and neck. *Nanomedicine: Nanotechnology, Biology and Medicine*, 42:102546, 2022, doi:10.1016/J.NANO.2022.102546.

[23] A. Christenhusz, A. E. Dassen, M. C. van der Schaaf, S. Salamzadeh, M. Brinkhuis, B. t. Haken, and L. Alic. Magnetic procedure for sentinel lymph node detection and evaluation of metastases: design and rationale of the Lowmag trial. *BMC Methods 2024 1:1*, 1(1):1–13, 2024, doi:10.1186/S44330-024-00006-3.

[24] N. S. Cheng. Formula for the Viscosity of a Glycerol-Water Mixture. *Industrial and Engineering Chemistry Research*, 47(9):3285–3288, 2008, doi:10.1021/IE071349Z.

[25] R. Burton-Opitz and R. Nemser. The viscosity of lymph. *American Journal of Physiology*, 45(1):25–29, 1917, doi:10.1152/AJPLEGACY.1917.45.1.25.

[26] Y. Tang, B. Liu, Y. Zhang, Y. Liu, Y. Huang, and W. Fan. Interactions between nanoparticles and lymphatic systems: Mechanisms and applications in drug delivery. *Advanced Drug Delivery Reviews*, 209:115304, 2024, doi:10.1016/J.ADDR.2024.115304.

[27] D. F. Williams, C. M. Wang, and U. Arz. In-phase/quadrature covariance-matrix representation of the uncertainty of vectors and complex numbers. *2006 68th ARFTG Conference on Measurement for Emerging Technologies, ARFTG 2006*, 2006, doi:10.1109/ARFTG.2006.8361655.

[28] D. B. Reeves and J. B. Weaver. Simulations of magnetic nanoparticle Brownian motion. *Journal of Applied Physics*, 112(12), 2012, doi:10.1063/1.4770322/354506.

[29] H. Rogge, M. Erbe, T. M. Buzug, and K. Lüdtke-Buzug. Simulation of the magnetization dynamics of diluted ferrofluids in medical applications. *Biomedizinische Technik*, 58(6):601–609, 2013, doi:10.1515/bmt-2013-0034.

[30] P. Arosio, F. Orsini, F. Brero, M. Mariani, C. Innocenti, C. Sangregorio, and A. Lascialfari. The effect of size, shape, coating and functionalization on nuclear relaxation properties in iron oxide core–shell nanoparticles: a brief review of the situation. *Dalton Transactions*, 52(12):3551–3562, 2023, doi:10.1039/D2DT03387A.

[31] M. Utkur, Y. Muslu, and E. U. Saritas. Relaxation-based viscosity mapping for magnetic particle imaging. *Physics in Medicine & Biology*, 62(9):3422, 2017, doi:10.1088/1361-6560/62/9/3422.

[32] Suriyanto, E. Y. Ng, and S. D. Kumar. Physical mechanism and modeling of heat generation and transfer in magnetic fluid hyperthermia through Néelian and Brownian relaxation: a review. *BioMedical Engineering OnLine 2017 16:1*, 16(1):1–22, 2017, doi:10.1186/S12938-017-0327-X.

[33] L. He, L. Wenzhong, Q. Xie, S. Pi, and P. C. Morais. A fast and remote magnetonanothermometry for a liquid environment. *Measurement Science and Technology*, 27(2):025901, 2015, doi:10.1088/0957-0233/27/2/025901.

[34] K. J. Janssen, J. Zhong, T. Viereck, M. Schilling, and F. Ludwig. Quantitative temperature visualization with single harmonic-based magnetic particle imaging. *Journal of Magnetism and Magnetic Materials*, 563:169915, 2022, doi:10.1016/J.JMMM.2022.169915.

